

DIFFERENT TYPES OF ULTRALUMINOUS X-RAY SOURCES IN NGC 4631

ROBERTO SORIA¹, AND KAJAL K. GHOSH²

Submitted to ApJ on 2008 September 2. Accepted 2009 January 27.

ABSTRACT

We have re-examined the most luminous X-ray sources in the starburst galaxy NGC 4631, using *XMM-Newton*, *Chandra* and *ROSAT* data. The most interesting source is a highly variable supersoft ULX. We suggest that its bolometric luminosity \sim a few 10^{39} erg s⁻¹ in the high/supersoft state: this is an order of magnitude lower than estimated in previous studies, thus reducing the need for extreme or exotic scenarios. Moreover, we find that this source was in a non-canonical low/soft ($kT \sim 0.1$ – 0.3 keV) state during the *Chandra* observation. By comparing the high and low state, we argue that the spectral properties may not be consistent with the expected behaviour of an accreting intermediate-mass black hole. We suggest that recurrent super-Eddington outbursts with photospheric expansion from a massive white dwarf ($M_{\text{wd}} \gtrsim 1.3M_{\odot}$), powered by non-steady nuclear burning, may be a viable possibility, in alternative to the previously proposed scenario of a super-Eddington outflow from an accreting stellar-mass black hole. The long-term average accretion rate required for nuclear burning to power such white-dwarf outbursts in this source and perhaps in other supersoft ULXs is ≈ 5 – $10 \times 10^{-6}M_{\odot} \text{ yr}^{-1}$: this is comparable to the thermal-timescale mass transfer rate invoked to explain the most luminous hard-spectrum ULXs (powered by black hole accretion). The other four most luminous X-ray sources in NGC 4631 (three of which can be classified as ULXs) appear to be typical accreting black holes, in four different spectral states: high/soft, convex-spectrum, power-law with soft excess, and simple power-law. None of them requires masses $\gtrsim 50M_{\odot}$.

Subject headings: X-rays: binaries — X-rays: individual (NGC 4631) — black hole physics

1. INTRODUCTION

The most luminous non-nuclear X-ray sources in nearby galaxies occur in regions of current or recent star formation. Some of them have X-ray luminosities exceeding the isotropic Eddington luminosity L_{Edd} for an $\approx 10M_{\odot}$ black hole (BH); they are commonly labelled ultraluminous X-ray sources (ULXs). The conservative interpretation is that the large majority of ULXs are the upper end of the high-mass X-ray binary population, powered by an accreting BH formed from “normal” stellar processes. If so, their (apparent) extreme luminosity is due to any of the following three reasons, or to a combination of them: moderately anisotropic emission (King et al. 2001; King 2008); mildly super-Eddington luminosities (Begelman 2002, 2006; Ohsuga & Mineshige 2007); extremely heavy stellar-mass BHs, with masses ~ 30 – $70M_{\odot}$ (Pakull & Mirioni 2002). Those scenarios also require mass accretion rates $\dot{m} \gtrsim 1$, where the accretion parameter $\dot{m} \equiv \dot{M}/\dot{M}_{\text{Edd}} \approx (0.1c^2\dot{M})/L_{\text{Edd}}$. Alternatively, there is still room for the more intriguing hypothesis that at least some ULXs are powered by intermediate-mass BHs (Miller & Colbert 2004).

In the absence of direct kinematic measurements (because of the faintness of their optical counterparts), X-ray spectral and timing studies have been used to try and constrain BH masses in ULXs. Such model-dependent arguments rely on the (expected) simple scaling of characteristic variability timescales and disk temperatures with BH mass, and on the correspondence of ULX spec-

tral states with the “canonical” states of Galactic BHs, for which the mass is accurately known. Unfortunately, ULXs do not appear to have the same state-transition behavior as Galactic BHs; for example, the most luminous sources are rarely found in a high/soft state, dominated by a standard accretion disk (Soria & Kuncic 2008). The X-ray spectra of some ULXs are dominated by an unbroken power law, with photon index $\Gamma \sim 1.5$ – 2 , whose physical origin is still unclear. Others have a broad component with a steepening or downward curvature above ~ 5 keV and sometimes a small soft excess below ~ 0.5 keV; this kind of spectrum may come from a slim disk, or from the inner region of a standard disk, heavily modified by Comptonization when $\dot{m} \gtrsim 1$. However, there is no clear gap between the two kinds of spectra, and the phenomenological classification of a source in either class usually depends on the signal-to-noise ratio available in the observations.

A small subsample of ULXs stands out from this general spectral classification: they have a thermal spectrum with temperatures $\lesssim 0.1$ keV and no emission above 1 keV. This is similar to the spectrum of classical supersoft sources in the Milky Way and Magellanic Clouds, but their luminosity is one or two orders of magnitude higher. The two most luminous supersoft ULXs are M101 ULX-1 (Kong & Di Stefano 2005) and NGC 4631 X1 (Carpano et al. 2007). Both sources are strongly variable or transient; when in a high state, their blackbody luminosity is $\sim 10^{40}$ erg s⁻¹. Other supersoft ULXs reaching bolometric luminosities $\gtrsim 10^{39}$ erg s⁻¹ have been found in M81 (Swartz et al. 2002), in the Antennae (Fabbiano et al. 2003) and (two) in NGC 300 (Carpano et al. 2006; Kong & Di Stefano 2003). Their thermal spectra can, in principle, provide tighter constraints on the size of the emitting region, and hence more significant tests for the

¹ Mullard Space Science Laboratory, University College London, Holmbury St Mary, Dorking, Surrey RH5 6NT. Email: roberto.soria@mssl.ucl.ac.uk

² Universities Space Research Association, NASA Marshall Space Flight Center, VP62, Huntsville, AL 35805, USA

geometry of the accretion flow and the nature and mass of the accretor.

While ULXs with a harder (power-law-like, slim-disk or Comptonized) X-ray spectrum may be interpreted as the upper end or the natural extension (either in BH mass or accretion rate) of stellar-mass BHs, supersoft ULXs appear like the upper end of nuclear-burning white dwarfs, which cannot be more massive than $\approx 1.4M_{\odot}$. Therefore, their high apparent luminosities are even more difficult to explain. The white dwarf scenario may be salvaged if supersoft ULXs are seen in a transient outburst phase, well above the Eddington luminosity of a white dwarf ($\sim 10^{38}$ erg s $^{-1}$). The other main competing scenarios for the emitting region in supersoft ULXs are a strong outflow from a stellar-mass BH accreting at a super-Eddington rate ($\dot{m} \gg 1$), or a standard disk around an intermediate-mass BH. For the disk to be so cool ($kT_{\text{in}} \lesssim 0.1$ keV), the BH mass needs to be $\gtrsim 10^4 M_{\odot}$.

In this paper, we re-examine the physical interpretation of the supersoft ULX in NGC 4631, by comparing the *XMM-Newton* observations taken when the source was in a more luminous state, with earlier *Chandra* observations in a lower state. We also discuss the physical nature of the other four most luminous X-ray sources in the *XMM-Newton* dataset.

2. OBSERVATIONS AND DATA ANALYSIS

NGC 4631 is a late-type starburst galaxy (Hubble type SB(s)d), seen nearly edge-on (Figure 1), at a distance of 7.6 Mpc (Seth, Dalcanton & de Jong 2005). In addition to a large number of giant starforming complexes, outflows and hot gas above the disk plane (Strickland et al. 2004a,b; Wang et al. 2001). From its integrated far-infrared luminosity, its star-formation rate is $\approx 3M_{\odot}$ yr $^{-1}$ (Strickland et al. 2004a; Soifer et al. 1989; Kennicutt 1998). In the X-ray band, NGC 4631 was studied with *Einstein* (Fabbiano, Kim & Trinchieri 1992), *ROSAT* (Vogler & Pietsch 1996; Read, Ponman & Strickland 1997; Liu & Bregman 2005), *Chandra* (Wang et al. 2001) and *XMM-Newton* (Tüllmann et al. 2006a,b; Feng & Kaaret 2005; Winter, Mushotzky & Reynolds 2006, 2007; Carpano et al. 2007). Here, we focus on the five brightest point-like sources in the *XMM-Newton* dataset (including four ULXs), and in particular on the supersoft ULX (Carpano et al. 2007), whose nature is still controversial.

Chandra observations of NGC 4631 with the Advanced CCD Imaging Spectrometer (ACIS) were carried out on 2000 April 16, for 60 ks (ObsID 797; Principal Investigator: Daniel Wang). We retrieved the data from the public archive, and analysed them with the locally-developed software tool LEXTRCT (Tennant 2006). Source detection in LEXTRCT was performed using a circular Gaussian approximation to the point spread function (PSF), which gives higher weight to sources with a central concentration of events. Point-source counts and spectra were extracted from within the 95% encircled-energy aperture of the model PSF. The background was extracted from annular regions surrounding the sources, except in crowded regions of the field where we used background regions adjacent to the sources. The background-subtracted counts within the source regions were scaled to obtain the aperture-corrected count values. The

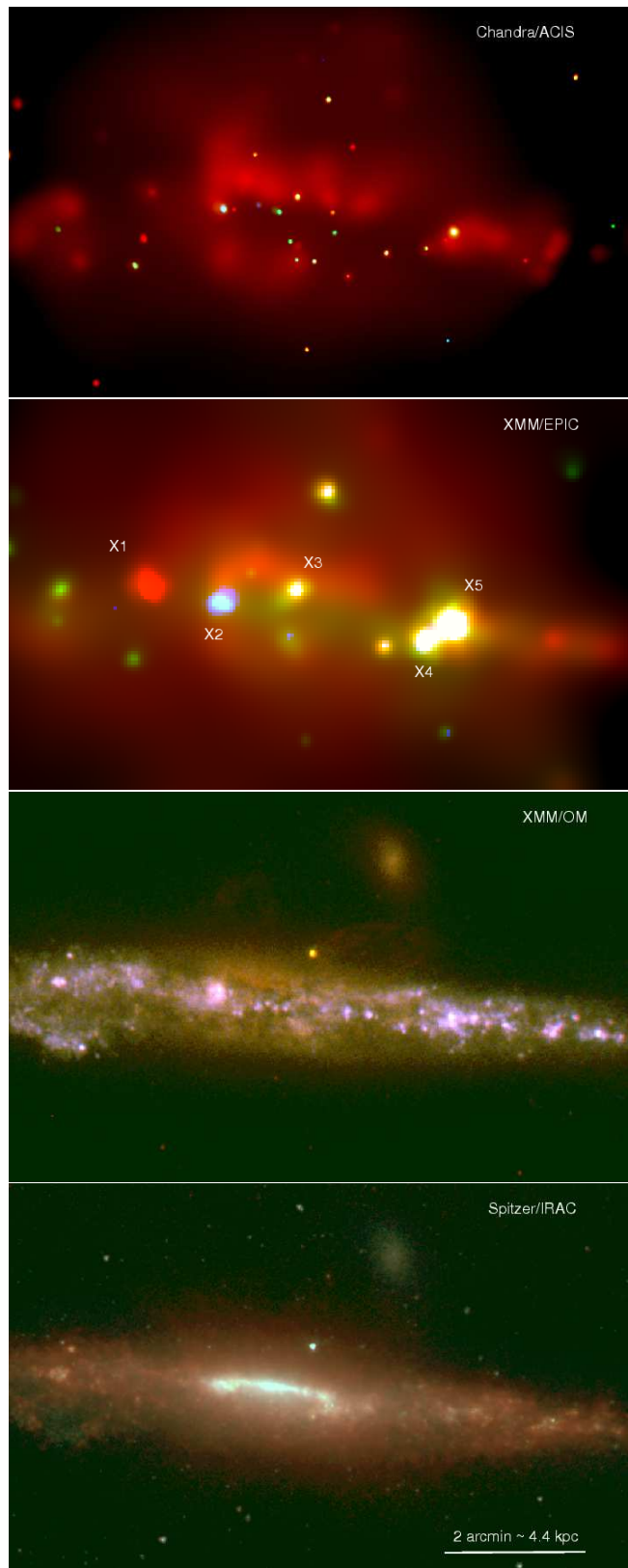


FIG. 1.— Multi-band view of NGC 4631. The true-color images from top to bottom are: *Chandra*/ACIS (red = 0.3–1 keV; green = 1–2 keV; blue = 2–8 keV); *XMM-Newton*/EPIC (red = 0.25–1 keV; green = 1–2 keV; blue = 2–10 keV), *XMM-Newton*/OM (red = *U* filter; green = *UVW1* filter; blue = *UVW2* filter); *Spitzer*/IRAC (red = 5.8 μm ; green = 4.5 μm ; blue = 3.6 μm). The five brightest sources in *XMM-Newton*, labelled X1 through X5, are the target of our study. In all images, North is up and East is left.

TABLE 1
LUMINOUS X-RAY SOURCES IN NGC 4631

| Source ID | ROSAT ID | R.A. | | Dec. | | Emitted Luminosity ^{ab} (erg s ⁻¹) | | | |
|-----------|----------|-------------|------------|------------------------------------|------------------------------------|---|------------------------------------|-------------------|--------------------|
| | | | | | | <i>Chandra</i> /ACIS | <i>XMM-Newton</i> /EPIC | <i>ROSAT</i> /HRI | <i>ROSAT</i> /PSPC |
| X1 | H13 | 12 42 15.96 | 32 32 49.4 | $\sim 10^{37}$ | $3.6_{-0.9}^{+0.5} \times 10^{39}$ | $5.7_{-1.5}^{+1.5} \times 10^{39}$ | $6.7_{-1.8}^{+1.8} \times 10^{39}$ | | |
| X2 | - | 12 42 11.13 | 32 32 35.8 | $4.0_{-0.3}^{+0.3} \times 10^{39}$ | $3.1_{-0.2}^{+0.2} \times 10^{39}$ | - | - | | |
| X3 | - | 12 42 06.07 | 32 32 46.5 | $3.9_{-0.2}^{+0.2} \times 10^{38}$ | $4.0_{-0.2}^{+0.2} \times 10^{38}$ | - | - | | |
| X4 | H8 | 12 41 57.35 | 32 32 03.2 | $3_{-1}^{+1} \times 10^{37}$ | $2.1_{-0.2}^{+0.2} \times 10^{39}$ | $9_{-2}^{+2} \times 10^{38}$ | $9_{-2}^{+2} \times 10^{38}$ | | |
| X5 | H7 | 12 41 55.56 | 32 32 16.9 | $3.8_{-0.1}^{+0.1} \times 10^{39}$ | $5.0_{-0.2}^{+0.2} \times 10^{39}$ | $3.5_{-0.3}^{+0.3} \times 10^{39}$ | $2.9_{-0.4}^{+0.4} \times 10^{39}$ | | |

^a For the supersoft source X1: bolometric luminosity ($E > 13.5$ eV); for the other sources: unabsorbed luminosity in the 0.3–10 keV band.
^b The error ranges listed for *Chandra* and *XMM-Newton* luminosities come from our spectral fitting; the error ranges for *ROSAT* luminosities include only the Poisson uncertainty in the HRI and PSPC count rates, after assuming the *XMM-Newton* best-fitting model for counts-to-flux conversion.

TABLE 2
EXTRAPOLATED BOLOMETRIC LUMINOSITY OF X1 FOR DIFFERENT FITTING MODELS

| XSPEC model | χ^2_ν | kT_{bb} (eV) | L_{bol} (erg s ⁻¹) |
|--|---------------|-----------------------|---|
| phabs _{Gal} *phabs*bb | 2.20(87.9/40) | 70_{-10}^{+11} | 1.5×10^{41} |
| phabs _{Gal} *phabs*(bb+gauss) | 1.40(52.0/37) | 69_{-4}^{+4} | 4.5×10^{40} |
| phabs _{Gal} *phabs*(bb+ray) | 1.80(68.3/38) | 78_{-11}^{+12} | 3.6×10^{39} |
| phabs _{Gal} *phabs*(bb+ray)*zedge | 1.23(44.3/36) | 91_{-9}^{+7} | 3.6×10^{39} |
| phabs _{Gal} *(ray+phabs*bb) | 1.50(57.0/38) | 66_{-23}^{+14} | 2.0×10^{40} |
| phabs _{Gal} *(ray+phabs*bb)*zedge | 1.24(44.6/36) | 85_{-10}^{+6} | 5.4×10^{39} |

background-subtracted point-source detection limit is 14 counts for the 2.8 minimum signal-to-noise ratio (S/N) threshold and a minimum 5 σ above background. For timing analysis, we binned the X-ray light curves of the brightest sources into 1000-s bins, and computed χ^2 tests against a constant flux hypothesis. For spectral analysis, we generated spectral redistribution matrices and ancillary response files with the *Chandra* X-ray Center software CIAO version 3.4. We then used XSPEC version 12.0 (Arnaud 1996) to fit the point-source spectra.

A 55-ks *XMM-Newton* observation with the European Photon Imaging Camera (EPIC) was carried out on 2002 June 28 (ObsID 0110900201; Principal Investigator: Michael Watson). We downloaded the public-archive data and processed them with the *XMM-Newton* Science Analysis System (SAS) version 6.5.0. We used LEXTRCT for source detection, and standard XMMSELECT tasks within the SAS for source and background region extraction. The radius of the source extraction regions was 20'', except for X4, where we used a 15'' radius to reduce contaminations from the nearby brighter source X5. Background extraction regions were chosen around the source regions, in a suitable way to avoid contamination. After building response and ancillary response files with rmfgen and arfgen we used XSPEC for spectral analysis of the brightest sources (Table 1). To improve the signal-to-noise ratio, we co-added the EPIC pn and MOS spectra, with suitably averaged response functions, using the method of Page et al. (2003).

To investigate the long-term variability of the ULXs, we also re-analyzed the archival *ROSAT*/HRI and PSPC observations carried out between 1991 December and 1992 December (Vogler & Pietsch 1996; Read, Ponman & Strickland 1997). We applied astrometric corrections to the *ROSAT* data using the *Chandra* source positions. We extracted source counts from circular regions of 30'' radius, and background counts from source-free circular regions of 3' radius. We used WebPIMMS with the best-fitting spectral parameters from the *XMM-Newton* study to convert *ROSAT* source count rates into fluxes. Three (X1=H13, X4=H8, and X5=H7; see Table 1 and Vogler & Pietsch (1996)) of the five luminous targets of this study were also found in *ROSAT*, with some variability over the various exposures.

3. THE SUPERSOFT ULX

X1 was detected as a luminous supersoft source during the *ROSAT*/PSPC observations of 1991 December 15 – 1992 January 04 (a total of 18.4 ks; see Fig. 4 and Table 1 in Vogler & Pietsch (1996)). It was not detected in the shorter (3.5 ks) *ROSAT*/PSPC observations of 1992 May, suggesting a count-rate decline by at least a factor of 3. It was detected again by *ROSAT*/HRI in 1992 December; however, since the HRI does not provide spectral information, we cannot tell whether it was again in a supersoft state. In the *Chandra* observation from 2000 April 16, the source was faint and soft. Finally, in the *XMM-Newton* observations of 2002 June 28, X1 appeared again

TABLE 3
BEST-FIT PARAMETERS FOR THE COADED EPIC PN AND MOS SPECTRUM OF X1 IN ITS HIGH/SUPERSOFT STATE. SPECTRAL MODEL: `phabs*phabs*(raymond-smith + bbody)*zedge`. VALUES IN BRACKETS WERE FIXED. ERRORS ARE 90% CONFIDENCE LEVELS FOR 1 INTERESTING PARAMETER ($\Delta\chi^2 = 2.7$).

| Parameter | <i>XMM-Newton</i> Value |
|-----------------------------------|-------------------------------------|
| $N_{\text{H,Gal}}^{\text{a}}$ | (1.3×10^{20}) |
| N_{H} | $2.4^{+0.3}_{-0.3} \times 10^{21}$ |
| kT_{rs} (keV) | $0.44^{+0.06}_{-0.06}$ |
| $Z(Z_{\odot})$ | (1.0) |
| K_{rs}^{b} | $9.2^{+1.9}_{-2.0} \times 10^{-6}$ |
| kT_{bb} (keV) | $0.091^{+0.07}_{-0.09}$ |
| K_{bb}^{c} | $5.7^{+0.5}_{-0.5} \times 10^{-6}$ |
| E_{edge} (keV) | $1.01^{+0.01}_{-0.07}$ |
| τ_{edge} | $2.0^{+1.2}_{-0.7}$ |
| χ^2/dof | 1.23(44.3/36) |
| $f_{0.3-10}^{\text{d}}$ | $3.3^{+0.1}_{-0.1} \times 10^{-14}$ |
| $f_{0.3-10,\text{rs}}^{\text{e}}$ | $8.4^{+2.1}_{-1.8} \times 10^{-15}$ |
| f_{1-10}^{f} | $1.4^{+0.1}_{-0.1} \times 10^{-15}$ |
| $f_{1-10,\text{rs}}^{\text{g}}$ | $1.0^{+0.2}_{-0.2} \times 10^{-15}$ |
| $L_{\text{bol}}^{\text{h}}$ | $3.6^{+0.9}_{-0.5} \times 10^{39}$ |
| $L_{\text{bol,rs}}^{\text{i}}$ | $2.6^{+0.7}_{-0.5} \times 10^{38}$ |

^aFrom Kalberla et al. (2005). Units of cm^{-2} .

^bRaymond-Smith model normalization $K_{\text{rs}} = 10^{-14}/\{4\pi [d_A (1+z)]^2\} \int n_e n_H dV$, where d_A is the angular size distance to the source (cm), n_e is the electron density (cm^{-3}), and n_H is the hydrogen density (cm^{-3}).

^cBlackbody model normalization $K_{\text{bb}} = L_{39}/D_{10}^2$ where L_{39} is the source luminosity in units of $10^{39} \text{ erg s}^{-1}$ and D_{10} is the distance in units of 10 kpc.

^dObserved flux in the 0.3–10 keV band; units of $\text{erg cm}^{-2} \text{ s}^{-1}$.

^eObserved flux in the 0.3–10 keV band, in the Raymond-Smith component; units of $\text{erg cm}^{-2} \text{ s}^{-1}$.

^fObserved flux in the 1–10 keV band; units of $\text{erg cm}^{-2} \text{ s}^{-1}$.

^gObserved flux in the 1–10 keV band, in the Raymond-Smith component; units of $\text{erg cm}^{-2} \text{ s}^{-1}$.

^hUnabsorbed luminosity for $E > 13.6 \text{ eV}$; units of erg s^{-1} .

ⁱUnabsorbed luminosity for $E > 13.6 \text{ eV}$, in the Raymond-Smith component; units of erg s^{-1} .

as a luminous supersoft source (Carpano et al. 2007), in a similar state to the 1991 detection. Here, we briefly summarize the spectral results when the source was in a high state, and then compare them with the low-state observation.

3.1. High state

We re-extracted the *XMM-Newton* data and coadded the pn and MOS spectra with a suitably averaged response function. This is equivalent to fitting them simultaneously, but provides a better signal-to-noise ratio for discrete features. We recover the result of Carpano et al. (2007), with a spectrum dominated by a soft black-

body component, plus residual features (both in emission and absorption) especially at $\approx 0.7\text{--}1.2 \text{ keV}$ (Figure 2). Such features are already evident in each individual EPIC spectrum, as plotted in Figure 4 of Carpano et al. (2007), and become more significant when the spectra from all three detectors are combined. The visual impression of such systematic residuals is confirmed by the fit statistics: the best-fitting absorbed blackbody model has $\chi^2 = 2.20(87.9/40)$ and can be safely rejected.

The residual emission and absorption features may not seem to affect the bolometric luminosity significantly, compared with the dominant blackbody emission. However, different models for such residual components have the effect of shifting the fitted temperature of the blackbody component between ≈ 65 and 90 eV , with a dramatic effect on the extrapolated, unabsorbed bolometric luminosity. Some examples are summarized in Table 2. When we model the deviations from a pure blackbody spectrum with only emission components (e.g., a Gaussian as in Carpano et al. (2007), or an optically-thin thermal plasma), we find an extrapolated luminosity $\approx 2\text{--}5 \times 10^{40} \text{ erg s}^{-1}$. However, we also find that there is a statistically-significant absorption feature at $E = 1.0 \pm 0.1 \text{ keV}$. This may be analogous to the Fe-L absorption edges found in some Seyfert galaxies (Boller et al. 2003). Ignoring this edge leads to apparently lower blackbody temperatures and therefore higher extrapolated bolometric luminosities. When we include this edge in our models (Tables 2 and 3), we obtain bolometric luminosities as low as $\approx 4\text{--}5 \times 10^{39} \text{ erg s}^{-1}$, depending on whether we assign the same, high intrinsic absorption to both the optically-thin and optically-thick thermal components, or only to the latter. On the other hand, the isotropic emitted luminosity $2 \times 10^{39} \text{ erg s}^{-1}$ in the 0.3–10 keV band provides a solid lower limit to the bolometric luminosity.

In our best-fitting model (Table 3), the optically-thin emission component contributes less than 1/10 of the extrapolated bolometric luminosity, but about 1/4 of the observed flux in the full 0.3–10 keV band, about half of the unabsorbed luminosity at energies $> 0.7 \text{ keV}$, and 2/3 of the unabsorbed luminosity at energies $> 1 \text{ keV}$. This explains why modelling such component has a great effect on the fit parameters and inferred luminosity. The unabsorbed luminosity of the optically-thin thermal plasma is $\approx 2.0 \times 10^{38} \text{ erg s}^{-1}$ (bolometric luminosity $\approx 2.6 \times 10^{38} \text{ erg s}^{-1}$).

The 1991 *ROSAT*/PSPC spectrum is also dominated by a blackbody component at $kT_{\text{bb}} \lesssim 0.1 \text{ keV}$ (Read, Ponman & Strickland 1997), and a *WebPIMMS* estimate suggests it may have similar luminosity to the 2002 *XMM-Newton* spectrum. However, the *ROSAT* data do not have enough counts and spectral resolution to constrain the temperature (and therefore the extrapolated emitted luminosity) more accurately. If we assume that the spectral model was the same as in the *XMM-Newton* observation (choosing for example the model listed in Table 3), and leave only the relative normalization free between the two epochs, we find that the two spectra are indeed consistent with being very similar (Figure 3), with a *ROSAT* flux normalization $1.33^{+0.33}_{-0.30}$ times higher than for *XMM-Newton*.

The best-fit blackbody temperature ($kT_{\text{bb}} = 0.09 \pm$

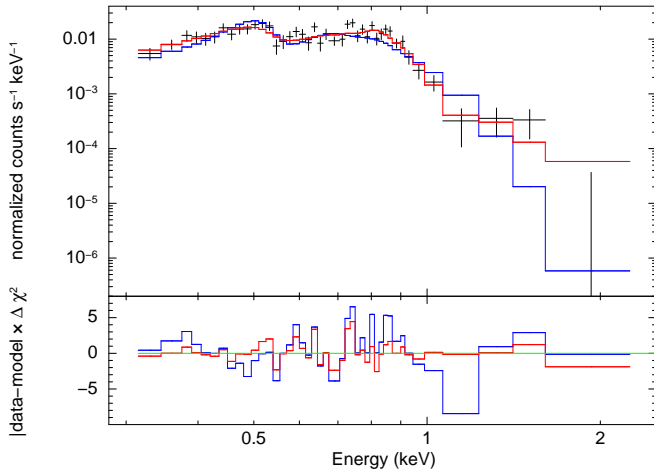


FIG. 2.— Model fits and χ^2 residuals for the combined *XMM-Newton*/EPIC spectrum of X1: simple blackbody (blue curve; $\chi^2_{\nu} \approx 2.2$), and blackbody plus thermal-plasma emission plus absorption edge (red curves; $\chi^2_{\nu} \approx 1.2$; best-fitting parameters in Table 3).

0.01 keV) and (extrapolated) blackbody luminosity ($L_{\text{bb}} \approx 4 \times 10^{39}$ erg s $^{-1}$ in 2002, and $\approx 5 \times 10^{39}$ erg s $^{-1}$ in 1991) correspond to a characteristic radius $\approx 2.1 \times 10^9$ cm or $\approx 2.4 \times 10^9$ cm (in 2002 and 1991, respectively) for the optically-thick emitting surface. We should also keep in mind that a simple blackbody approximation tends to overestimate the true luminosity of supersoft sources by a factor of a few (Kahabka & van den Heuvel 1997), so the true luminosity may be even lower.

3.2. Low state

From the *Chandra* data in the low state, we found ≈ 13.5 net ACIS counts, corresponding to a count rate of $(2.3 \pm 0.7) \times 10^{-4}$ ct s $^{-1}$ (a factor of two less than estimated by Carpano et al. (2007)). The breakdown of the net counts in different energy bands is: ≈ 12.2 counts at 0.3–1.5 keV, and ≈ 1.3 counts at 1.5–8.0 keV. Dividing the interval into three bands, we get: ≈ 10 counts at 0.3–1.0 keV, ≈ 2.5 counts at 1.0–2.0 keV, $\lesssim 1$ counts at 2.0–8.0 keV.

So, although there are not enough counts for detailed spectral fitting, we have at least a strong indication that the source was very soft (or “quasi-soft” in the definition of Di Stefano & Kong (2004)). Even if we assume no intrinsic absorption, the count distribution rules out a power-law spectrum with photon index $\Gamma \lesssim 2$ at the 90 per cent confidence level (using the Cash statistic, Cash (1979)). The optically-thin thermal plasma component fitted to the high-state spectrum is clearly inconsistent with the lower flux detected in the low state (Figure 4). More generally, optically-thin thermal plasma models (at fixed solar metallicity) are also ruled out at the 90 per cent confidence level (the best-fitting model has a Cash-statistic parameter = 21.8/14) Soft, optically-thick thermal emission (blackbody or disk-blackbody) is a much better model for the observed count distribution. We estimate a disk-blackbody temperature $kT_{\text{in}} = 0.22^{+0.32}_{-0.13}$ keV (90 per cent confidence limits; Cash-statistic fit parameter = 13.6/14) or a simple blackbody temperature $kT_{\text{bb}} = 0.18^{+0.13}_{-0.10}$ keV (Cash-statistic fit parameter = 13.2/14). The best-fitting unabsorbed luminosity is

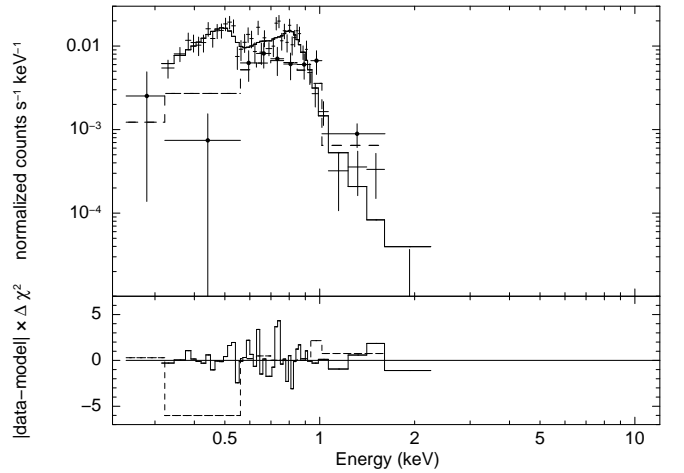


FIG. 3.— Combined fit to the *XMM-Newton*/EPIC (solid line) and *ROSAT*/PSPC (dashed line) binned spectra for the supersoft source X1 in its high state (datapoints and χ^2 residuals). The *XMM-Newton* data are from 2002 June; the *ROSAT* data from 1991 December – 1992 January. The main component of the best-fitting model (Table 3) is an absorbed blackbody with $kT_{\text{bb}} = 0.08 \pm 0.02$ keV; the normalization of the *ROSAT* spectrum is a factor ≈ 1.3 higher than that of the *XMM-Newton* spectrum.

$\approx 10^{37}$ erg s $^{-1}$, although the 68 per cent confidence interval includes values as high as $\approx 10^{38}$ erg s $^{-1}$; but in any case, the luminosity is lower than in the supersoft state, as intuitively expected from a simple scaling of the count rate between the *Chandra* and *XMM-Newton* observations. From the few detected counts, we cannot strongly rule out the alternative possibility that the lower count rate in the *Chandra* observation is also or mostly due to a much higher intrinsic absorption ($N_{\text{H}} \gtrsim 10^{22}$ cm $^{-2}$) of the same, luminous super-soft component. But in the absence of independent evidence for that dramatic change in absorption, and by analogy with the behaviour of other accreting systems (including the supersoft source in M101 mentioned earlier, Kong & Di Stefano (2005)), here we consider the low-state scenario as the most plausible.

The absence of the optically-thin thermal plasma component in low state is somewhat puzzling. The rapid change between 2000 and 2002 suggests that it was not due to diffuse hot gas at large distances from the source, but was instead directly associated with the high state or outburst. The PSF and source extraction region are of course much larger for *XMM-Newton*, which may suggest a contamination from Galactic-scale diffuse emission; however, we tested this possibility using the *Chandra* images, and we do not find evidence of local enhancements in the diffuse soft emission. Different choices of background extraction regions in *XMM-Newton* do not remove this component. In conclusion, we suggest that the most likely explanation at this stage is that the line emission and absorption edge are really associated with the compact source. If the emission is due to an expanding BH wind or white dwarf photosphere (scenarios outlined in Sections 4.2 and 4.3) we speculate that this may be evidence of an optically thick and optically thin component in the outflow.

4. PHYSICAL INTERPRETATION OF X1

Three scenarios have been considered for this source (and for the handful of similar ones in other nearby galax-

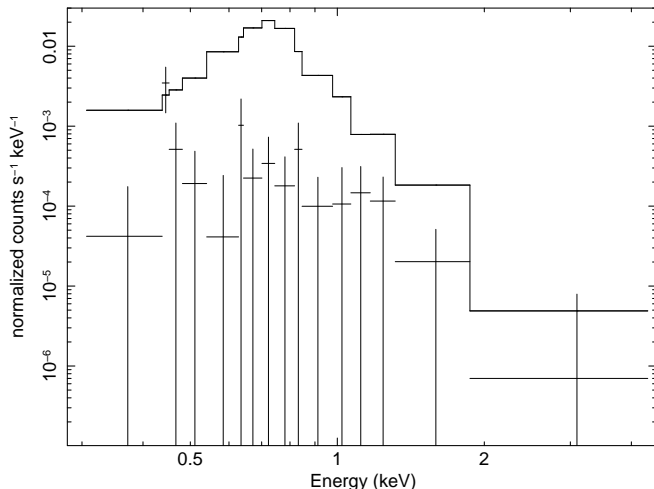


FIG. 4.— Datapoints from the *Chandra* observation in the low state (each bin corresponding to a single detected count) compared with the expected contribution from the optically-thin thermal component alone, using the best-fitting parameters of the high state (Table 3).

ies), based on the properties of its high/supersoft state (Carpano et al. 2007): standard disk emission from an intermediate-mass BH; super-Eddington outflows from a stellar-mass BH; nuclear-burning white dwarf. We discuss here how the low-state appearance provides stronger constraints.

4.1. Intermediate-mass BH

In the standard disk model, the BH mass can be expressed as a function of inner-disk temperature and bolometric disk luminosity (or diskbb normalization constant): $M \sim T_{\text{in}}^{-2} L_{\text{disk}}^{1/2}$ (Makishima et al. 2000). Assuming $R_{\text{in}} = 6M$ and imposing $N_{\text{H}} \geq 1.3 \times 10^{20} \text{ cm}^{-2}$ (Galactic line of sight), we used the Cash-statistics fit to the *Chandra* data, and we derived a contour plot of the acceptable region in the BH-mass versus disk-luminosity space (Figure 5). We do not have enough net counts to determine the 90% confidence contours, but we can at least identify a “most plausible” (68% confidence contours) region in that plane. The large uncertainty in the inner-disk temperature (from ~ 0.1 to ~ 0.5 keV) is reflected in a large range of masses and unabsorbed luminosities. Regardless of BH mass, the luminosity appears to be always $< 0.01 L_{\text{Edd}}$. However, there are observational and theoretical arguments against a disk-dominated low/soft state at $L < 0.01 L_{\text{Edd}}$. At those luminosities, accreting BHs are generally found in a power-law-dominated low/hard state, which is ruled out in this case. Hence, we suggest that the low/soft appearance of the source in the *Chandra* observation does not favour the disk-blackbody model.

Moreover, the fitted inner-disk temperature in the low/soft state appears to be similar or slightly higher than the thermal temperature in the high/supersoft state (Carpano et al. (2007), and Table 2). If the thermal emission is due to an accretion disk, we expect the disk to be cooler, when the net count rate (a proxy for the accretion rate and emitted luminosity) is two or three orders of magnitude lower; $T_{\text{in}} \sim L_{\text{disk}}^{1/4}$ in a standard disk. A transition between high/supersoft and low/soft

states is inconsistent with the well-studied behaviour of BH accretion disks. In conclusion, the comparison of low- and high-state spectral data does not favour the intermediate-mass BH scenario.

4.2. Stellar-mass BH

The high/supersoft state is consistent with thermal emission scattered and collimated by a massive, optically-thick disk outflow, launched at the spherization radius around a stellar-mass BH, when the accretion rate exceeds the Eddington limit (Shakura & Sunyaev 1973; Poutanen et al. 2007; King 2008). We have already noted that in the *Chandra* observation, the emitted luminosity may be two or three orders of magnitude lower. Hence, we do not expect the super-Eddington outflow to be present in that lower state.

In the canonical scheme of BH accretion states, inferred mostly from the study of stellar-mass Galactic BH binaries, moderately active (sub-Eddington) BHs are either in the high/soft state (dominated by a disk-blackbody component with $kT_{\text{in}} \approx 1$ keV), or in the low/hard state (power-law component with $\Gamma \sim 1.5$ –2). Neither state is consistent with the observed *Chandra* spectrum. And conversely, no stellar-mass BHs have been observed in a disk-dominated state with $kT_{\text{in}} \sim 0.2$ keV and $L_{\text{X}} \sim 10^{37}$ – $10^{38} \text{ erg s}^{-1}$. If the supersoft component in the higher state is attributed to a disk outflow during super-critical accretion, we would have to conclude that the lower-state spectrum does not look like a canonical state for stellar-mass BHs.

An alternative possibility we should consider is that the sequence of high and low states is not due to accretion state transitions, but to a long-term precession of the binary system, such that the moderately collimated outflow moves in and out of our line of sight. When we are looking down the outflow, we may be observing the undisturbed, cooler (soft spectrum) outer disk, at radii larger than the spherization radius. However, a difficulty of this interpretation is that the predicted isotropic luminosity of the outer standard disk down to the spherization radius should be $\approx L_{\text{Edd}} \approx 10^{39} \text{ erg s}^{-1}$ for a stellar-mass BH. This is much higher than observed.

In conclusion, we suggest that the stellar-mass BH scenario, although still viable, has not yet provided a perfectly self-consistent interpretation for this source, or at least requires a new kind of accretion-state behaviour or accretion-disk structure, so far unobserved in stellar-mass BHs.

4.3. Nuclear-burning white dwarf

The observed temperature and luminosity of X1 in the low/soft state is consistent with the thermal emission from surface hydrogen burning on a massive white dwarf, $M_{\text{wd}} \approx 1.3$ – 1.35 (Figure 6). Such process can occur at accretion rates just below the steady burning rate (\sim a few $10^{-7} M_{\odot} \text{ yr}^{-1}$: Starrfield et al. (2004); Kahabka (2004). The white dwarf is sufficiently hot that hydrogen burns on its surface immediately as it is accreted; for this reason, the system does not go through classical-nova outbursts. A blackbody luminosity $\approx 10^{38} \text{ erg s}^{-1}$ at a temperature $kT_{\text{bb}} \sim 0.1$ keV are well within the 68% confidence limit of the *Chandra* detection. These values correspond to a radius ~ 3000 km for a spherical emitter, consistent with the radius of a $1.35 M_{\odot}$ white dwarf.

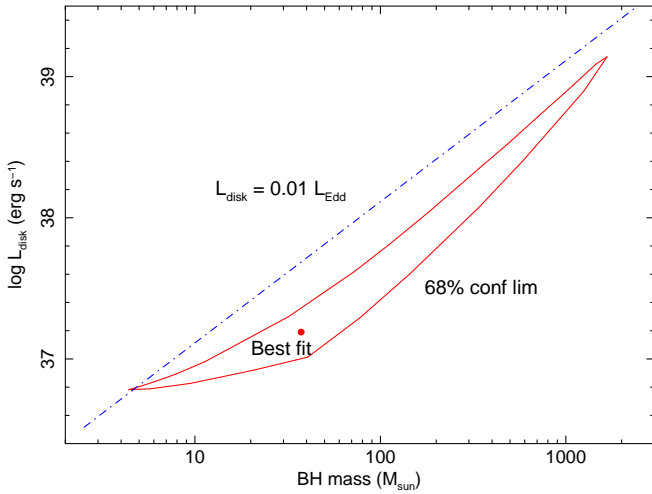


FIG. 5.— Contour plot for the 68% confidence region in the BH mass versus bolometric disk luminosity plane, for X1 in its low/soft state (*Chandra* observation), if its spectrum is fitted with an absorbed disk-blackbody. The dash-dotted line corresponds to $L_{\text{disk}} = 0.01 L_{\text{Edd}}$, a conventional threshold below which the disk is not expected to be the dominant emitting component in accreting BHs (and therefore a disk-blackbody model would not be self-consistent).

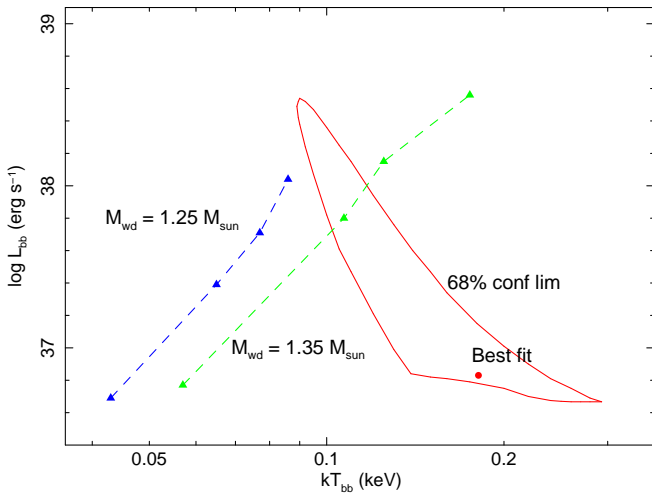


FIG. 6.— Contour plot for the 68% confidence region in the BH mass versus bolometric luminosity plane, for X1 in its low/soft state (*Chandra* observation), if its spectrum is fitted with an absorbed blackbody. The dashed lines correspond to the predicted effective temperatures and luminosities for massive white dwarfs ($1.25 M_{\odot}$ and $1.35 M_{\odot}$) during phases of surface hydrogen burning, for different values of mass accretion rates, increasing from $1.6 \times 10^{-8} M_{\odot} \text{ yr}^{-1}$ to $8.0 \times 10^{-7} M_{\odot} \text{ yr}^{-1}$ (see Starrfield et al. (2004) for detailed explanations of those sequences).

However, the high/supersoft phases cannot be explained with steady surface burning. It was found from numerical simulations (Starrfield et al. 2004) that steady surface hydrogen burning on a $1.35 M_{\odot}$ white dwarf can occur only for accretion rates $\lesssim 10^{-6} M_{\odot} \text{ yr}^{-1}$; above that limit, the photosphere of the white dwarf expands to large radii and shuts off accretion. This may be what is happening in X1, with a sequence of outbursts in between phases of more steady surface burning (at reduced accretion rate) or simply of surface cooling. The estimated radii (a factor of 10 higher than in the low/soft state, Section 3.1) and blackbody temperatures (a factor

of two lower) fitted to the high/supersoft spectrum are consistent with photospheric expansion.

From the sequence of X-ray observations between 1991 and 2002, we speculate that X1 is in a transient supersoft state about half of the time. Since the emitted luminosity in the high/supersoft state is \sim a few $10^{39} \text{ erg s}^{-1}$, and that in the low/soft state is \sim a few $10^{37} \text{ erg s}^{-1}$, the long-term average luminosity may be $\sim 2 \times 10^{39}$. This clearly raises two problems, related to the average long-term accretion rate and to the peak luminosity. Since all the power must ultimately come from nuclear burning, the long-term average luminosity requires an average accretion rate $\sim (0.5\text{--}1) \times 10^{-5} M_{\odot} \text{ yr}^{-1}$. From stellar evolution models (Rappaport, Podsiadlowski & Pfahl 2005), it appears that even late-type B stars (likely progenitor of the putative massive white dwarf and likely donor star in the system) can provide such extreme rates during thermal-timescale episodes of mass transfer, lasting $\sim 10^5 \text{ yr}$. If the same accretion rate was used to power an accreting BH, it would produce a bolometric luminosity $\sim (3\text{--}6) \times 10^{40} \text{ erg s}^{-1}$, which is similar to the maximum luminosity inferred for ULXs; the X-ray luminosity distribution of ULXs has a downturn at $L_X \approx 2 \times 10^{40} \text{ erg s}^{-1}$ (Grimm, Gilfanov & Sunyaev 2003; Swartz et al. 2004). In other words, explaining the most luminous supersoft sources ever found as nuclear-burning sources with average long-term luminosity $\sim 10^{39} \text{ erg s}^{-1}$ requires mass-transfer conditions similar to those needed to explain the most luminous ULXs as accreting BHs with luminosities \sim a few $10^{40} \text{ erg s}^{-1}$. We speculate that this may be more than a coincidence. Moreover, the alternative ULX scenario of a super-Eddington outflow from a stellar-mass BH (Section 4.2; Carpano et al. (2007); King (2008)) also requires mass transfer rates of up to $\approx 10^{-5} M_{\odot} \text{ yr}^{-1}$ on the thermal timescale, possibly from a B-type donor star. Therefore, the required limits on the long-term average mass transfer rate are similar for both models.

As for the peak luminosity \sim a few $10^{39} \text{ erg s}^{-1}$, this is highly super-Eddington for a white dwarf, and a factor of 10 above the luminosity produced by steady surface burning. However, steady burning cannot persist at accretion rates $\approx 10^{-5} M_{\odot} \text{ yr}^{-1}$. We speculate that the high/supersoft phases may be transient super-Eddington events (fireball scenario), after which the photosphere shrinks again to the white-dwarf surface, and accretion resumes. It was estimated (Starrfield et al. 2004) that the hydrogen layer involved in surface nuclear burning has a mass $\sim 10^{-6} M_{\odot}$. Therefore, even if further hydrogen accretion is shut off (i.e., during the transient super-Eddington outburst), simply the complete burning of this layer can provide a luminosity $\gtrsim 10^{39} \text{ erg s}^{-1}$ for several weeks, or $> 10^{40} \text{ erg s}^{-1}$ for several days, and the layer itself can be replenished in ~ 1 month, before another outburst. A similar process may be driving the outburst cycles of the supersoft ULX in M101 (Kong & Di Stefano 2005), which shows varying temperatures between ≈ 50 and $\approx 150 \text{ eV}$ corresponding perhaps to phases of photospheric expansion and contraction. Super-Eddington outbursts powered by non-steady episodes of nuclear burning have been observed in some Novae, most notably LMC 91, which peaked at $\approx 2.6 \times 10^{39} \text{ erg s}^{-1}$ (Schwarz et al. 2001).

In conclusion, we suggest that a fireball white-dwarf

model is still a viable scenario for this extreme source (and perhaps also for the whole class of supersoft ULXs), considering that its true bolometric luminosity is likely to be an order of magnitude less than originally estimated (Carpano et al. 2007), and that the required accretion rate $\approx 10^{-5} M_{\odot} \text{ yr}^{-1}$ is similar to the rate invoked for super-Eddington outflows in the most luminous ULXs.

4.4. Time variability

From a timing study of the *XMM-Newton* observation, it was found (Carpano et al. 2007) that the X-ray emission has a modulation with an apparent period of ≈ 4.1 hr. It is not clear what can produce this period or timescale. If it was the binary period, from the period-density relation (Warner 1995) we infer an average density $\approx 6 \text{ g cm}^{-3}$ inside the Roche lobe of the donor star (the mean solar density is $\approx 1.4 \text{ g cm}^{-3}$). This is consistent with a main-sequence star with a mass $\approx 0.5 M_{\odot}$. Other well-known supersoft sources such as CAL 87 are known to have a low-mass donor with a binary period of a few hours (Callanan et al. 1989). However, for NGC 4631 X1, such a low-mass donor is inconsistent with the required mass transfer rates in both the stellar-mass BH and white dwarf scenarios, and is also at odds with the young age of the stellar population in this starburst galaxy (i.e., the galaxy is more likely to contain bright high-mass X-ray binaries). A B-type donor star is consistent with a massive white-dwarf compact object, both from theoretical arguments (Iben & Tutukov 1994) and observationally (Berghöfer et al. 2000); the lifetime of the B-type progenitor of a $1.3 M_{\odot}$ white dwarf is $\approx 50 - 70$ Myr.

If the 4-hr X-ray modulation is not the binary period, then it could be due either to a disk precession in the BH scenario, or to the rotational period of the white dwarf, or to pulsations in the donor star which affect the rate of mass transfer. A study of these scenarios is beyond the scope of this work. We just point out that 4 hrs is the characteristic pulsation period of the B-type β -Cephei stars (Stankov & Handler 2005). Pulsations of a β -Cep donor have been invoked in the past as a possible cause of X-ray periodicities in some accreting binaries (Berghöfer et al. 2000; Finley et al. 1992).

5. OTHER LUMINOUS X-RAY SOURCES

5.1. X2

Apparently coincident with a young star cluster, this highly-absorbed ULX ($N_{\text{H}} \sim 2 \times 10^{22} \text{ cm}^{-2}$), was not detected in any *ROSAT* observation (not surprisingly). This source can be classified as a ‘‘convex-spectrum’’ ULX (using the terminology of Makishima (2007)). The spectral curvature can be formally modelled with a standard disk-blackbody spectrum (Figure 7 and Table 4), with a color temperature $kT_{\text{in}} \approx 1.3\text{--}1.5$ keV (in the *XMM-Newton* and *Chandra* data, respectively). However, as is generally the case in this class of ULXs, such temperatures are too high for the estimated luminosities (≈ 3 and $4 \times 10^{39} \text{ erg s}^{-1}$, respectively). One possibility is that the emission comes from a slim disk (Watarai, Mizuno & Mineshige 2001) rather than a standard disk; if so, the mass accretion rate may be an order of magnitude above the Eddington rate, while the luminosity may be $\sim L_{\text{Edd}}$, and the BH mass $\sim 20\text{--}30 M_{\odot}$ (for comparison with other sources in a similar state, see Fig. 3 in

TABLE 4
BEST-FITTING PARAMETERS FOR THE *Chandra*/ACIS AND *XMM-Newton*/EPIC SPECTRA OF X2. SPECTRAL MODEL: **wabs*wabs*diskbb**. VALUES IN BRACKETS WERE FIXED. ERRORS ARE 90% CONFIDENCE LEVELS FOR 1 INTERESTING PARAMETER ($\Delta\chi^2 = 2.7$).

| Parameter | <i>Chandra</i> Value | <i>XMM-Newton</i> Value |
|-------------------------------|-------------------------------------|-------------------------------------|
| $N_{\text{H,Gal}}^{\text{a}}$ | (1.3×10^{20}) | (1.3×10^{20}) |
| N_{H} | $28.3^{+3.6}_{-3.2} \times 10^{21}$ | $26.4^{+3.5}_{-3.2} \times 10^{21}$ |
| kT_{dbb} (keV) | $1.49^{+0.22}_{-0.18}$ | $1.26^{+0.11}_{-0.10}$ |
| $K_{\text{dbb}}^{\text{b}}$ | $5.8^{+4.5}_{-2.6} \times 10^{-3}$ | $8.5^{+4.5}_{-2.8} \times 10^{-3}$ |
| χ^2/dof | 0.65(42.4/65) | 0.78(42.1/54) |
| $f_{0.3-10}^{\text{c}}$ | $3.0^{+0.1}_{-0.2} \times 10^{-13}$ | $2.1^{+0.1}_{-0.2} \times 10^{-13}$ |
| $L_{0.3-10}^{\text{d}}$ | $4.0^{+0.3}_{-0.3} \times 10^{39}$ | $3.1^{+0.2}_{-0.2} \times 10^{39}$ |

^aFrom Kalberla et al. (2005). Units of cm^{-2} .

^b $K_{\text{dbb}} = [R_{\text{in}}(\text{km})/d(10 \text{ kpc})]^2 \times \cos \theta$ where R_{in} is the apparent inner-disk radius and θ the viewing angle; $\theta = 0$ is face-on.

^cObserved flux in the 0.3–10 keV band; units of $\text{erg cm}^{-2} \text{ s}^{-1}$.

^dUnabsorbed luminosity in the 0.3–10 keV band; units of erg s^{-1} .

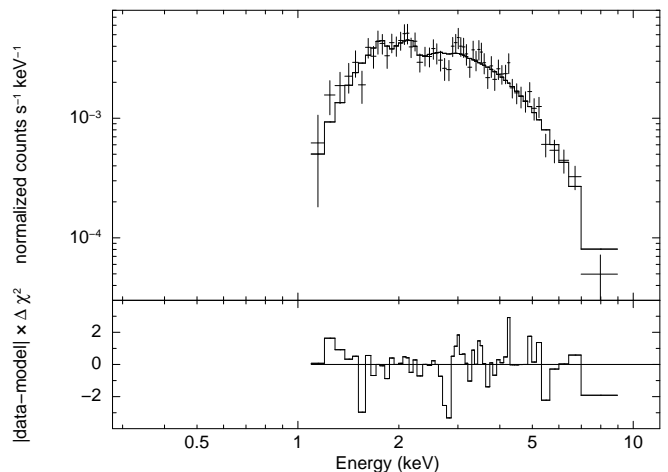


FIG. 7.— *XMM-Newton*/EPIC spectrum of X2 (datapoints and χ^2 residuals), fitted with a highly absorbed disk-blackbody model; see Table 4 for the best-fitting parameters.

Makishima (2007)). Alternatively, the convex spectrum may be modelled equally well with a Comptonized component, arising from a warm ($kT \sim 3\text{--}4$ keV) corona (see a comparison between the two scenarios in Stobbart et al. (2006)). Other purely phenomenological models such as a broken power-law (breaking at ~ 4 keV) also provide good fits.

5.2. X3

This X-ray source is also well modelled with a disk-blackbody spectrum (Figure 8 and Table 5), with $kT_{\text{in}} \approx 1.2\text{--}1.4$ keV (in the *XMM-Newton* and *Chandra* data, respectively), similar to the parameters found for X2. However, its emitted luminosity in the 0.3–10 keV band is only $\approx 4 \times 10^{38} \text{ erg s}^{-1}$, constant between *Chandra* and

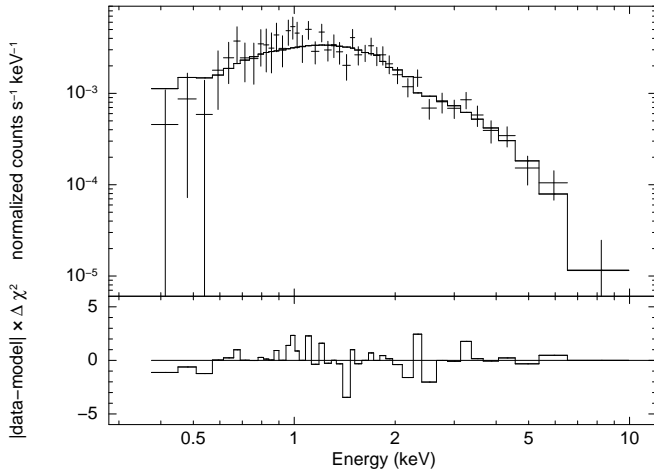


FIG. 8.— *XMM-Newton*/EPIC spectrum of X3 (datapoints and χ^2 residuals), fitted with a disk-blackbody model; see Table 5 for the best-fitting parameters.

XMM-Newton and below the *ROSAT* detection limit. Therefore, X3 is consistent with a stellar-mass BH near the upper-luminosity end of its high/soft state. Assuming a spectral hardening factor ≈ 1.7 –2 (Shimura & Takahara 1995; Gierliński & Done 2004; Shafee et al. 2006), the standard-disk temperature-luminosity relation (Makishima et al. 2000) suggests a BH mass ≈ 5 – $7M_{\odot}$; the fitted (apparent) inner-disk radius $R_{\text{in}} \approx 30(\cos\theta)^{-0.5}$ km, as expected.

5.3. X4

This ULX shows a state transition between the *Chandra* and *XMM-Newton* observations. In *Chandra*, we detect a faint, soft source (0.3–8 keV count rate = $(1.44 \pm 0.16) \times 10^{-3}$ counts s^{-1}), well fitted ($\chi^2_{\nu} = 0.88$) by an optically-thin thermal-plasma model (Table 6) with a temperature $kT_{\text{rs}} = 1.2^{+0.5}_{-0.2}$ keV. Every other spectral model (power-law, disk-blackbody, or any Comptonization models) yields $\chi^2_{\nu} \gtrsim 1.5$. The emitted luminosity for the Raymond-Smith thermal-plasma model is $\approx 3 \times 10^{37}$ erg s^{-1} . In the *XMM-Newton* observations, there is a stronger, harder source at the same position, with a broad spectrum well fitted by a power-law plus disk-blackbody model (Figure 9 and Table 6). The power-law index is $\Gamma \approx 1.9$; there is no evidence of a steepening break or spectral curvature near or above ~ 5 keV, unlike what we noted for X2. The disk-blackbody component has a color temperature $kT_{\text{in}} = 0.20^{+0.11}_{-0.05}$ keV. The unabsorbed luminosity in the 0.3–10 keV band is $(2.1 \pm 0.2) \times 10^{39}$ erg s^{-1} , ≈ 30 per cent of which in the disk-blackbody component. It is possible that the thermal-plasma component seen in the *Chandra* dataset is also present in the *XMM-Newton* spectrum, although we cannot place strong constraints on it (Table 6).

In summary, X4 is a transient “power-law” ULX (using again the spectral classification of Makishima (2007)) with a thermal soft-excess at low energies. A physical interpretation for this class of ULXs is that the standard optically-thick accretion disk is directly visible at large radii but is replaced or covered by a scattering-dominated region (producing a broader, power-law-like spectrum) at small radii (see, e.g., the review by Soria & Kuncic (2008) and references therein). The apparent inner-disk

TABLE 5
BEST-FITTING PARAMETERS FOR THE *Chandra*/ACIS AND *XMM-Newton*/EPIC SPECTRA OF X3. SPECTRAL MODEL: **wabs*wabs*diskbb**. VALUES IN BRACKETS WERE FIXED. ERRORS ARE 90% CONFIDENCE LEVELS FOR 1 INTERESTING PARAMETER ($\Delta\chi^2 = 2.7$).

| Parameter | <i>Chandra</i> Value | <i>XMM-Newton</i> Value |
|-------------------------------|-------------------------------------|-------------------------------------|
| $N_{\text{H,Gal}}^{\text{a}}$ | (1.3×10^{20}) | (1.3×10^{20}) |
| N_{H} | $2.0^{+1.0}_{-0.9} \times 10^{21}$ | $1.1^{+0.6}_{-0.5} \times 10^{21}$ |
| kT_{dbb} (keV) | $1.37^{+0.32}_{-0.21}$ | $1.20^{+0.17}_{-0.15}$ |
| $K_{\text{dbb}}^{\text{b}}$ | $7.8^{+6.9}_{-4.3} \times 10^{-4}$ | $13.8^{+9.2}_{-4.4} \times 10^{-4}$ |
| χ^2/dof | 0.81(17.9/22) | 0.75(30.7/41) |
| $f_{0.3-10}^{\text{c}}$ | $4.7^{+0.1}_{-0.1} \times 10^{-14}$ | $5.0^{+0.1}_{-0.1} \times 10^{-14}$ |
| $L_{0.3-10}^{\text{d}}$ | $3.9^{+0.2}_{-0.2} \times 10^{38}$ | $4.0^{+0.2}_{-0.2} \times 10^{38}$ |

^aFrom Kalberla et al. (2005). Units of cm^{-2} .

^b $K_{\text{dbb}} = [R_{\text{in}}(\text{km})/d(10 \text{ kpc})]^2 \times \cos\theta$ where R_{in} is the apparent inner-disk radius and θ the viewing angle; $\theta = 0$ is face-on.

^cObserved flux in the 0.3–10 keV band; units of $\text{erg cm}^{-2} \text{ s}^{-1}$.

^dUnabsorbed luminosity in the 0.3–10 keV band; units of erg s^{-1} .

radius (which we may identify with the transition radius between standard disk and Comptonizing regions) $R_{\text{in}} \approx 1600(\cos\theta)^{-0.5}$ km. From the relative contribution of thermal and (less radiatively efficient) power-law components, we speculate that this transition radius is \gtrsim a few times the innermost stable orbit; hence, the BH mass is likely to be $\lesssim 50M_{\odot}$.

Evidence of variability on monthly timescales for X4 was already found in the series of *ROSAT* observations (Vogler & Pietsch 1996). We searched for short-term variability in the *XMM-Newton* observation (Figure 10), and found that a constant count rate is statistically ruled out ($\chi^2_{\nu} = 117.2/83$). However, we found no dominant frequency or other spectral features in its power-density spectrum.

5.4. X5

This ULX was in a luminous state in five of the six *ROSAT* observations (Vogler & Pietsch 1996). We found it again in a bright state during the *Chandra* and *XMM-Newton* observations (Figure 11 and Table 7). In both datasets, the X-ray spectra are well fitted by a simple power-law of photon index $\Gamma \sim 2$. There is no statistically-significant evidence of either a soft thermal component or a high-energy break or downward curvature in the power-law. The unabsorbed isotropic luminosity in the 0.3–10.0 keV band is $(3.8 \pm 0.1) \times 10^{39}$ ergs s^{-1} (*Chandra*) and $(5.0 \pm 0.2) \times 10^{39}$ ergs s^{-1} (*XMM-Newton*, only slightly higher than the range of estimated luminosities during the *ROSAT* observations (Liu & Bregman 2005), when the same *Chandra* or *XMM-Newton* model is applied to the *ROSAT* data³. We did not find any variability within the individual *Chandra*

³ The *ROSAT*/HRI luminosity estimated by Liu & Bregman (2005) is a factor of 2 lower than our estimate because they assumed only line-of-sight absorption.

TABLE 6
BEST-FIT PARAMETERS FOR THE *Chandra*/ACIS AND *XMM-Newton*/EPIC SPECTRA OF X4. SPECTRAL MODEL: $wabs_1[(wabs_1 * raymond-smith) + wabs_2 * (power-law+diskbb)]$. VALUES IN BRACKETS WERE FIXED. ERRORS ARE 90% CONFIDENCE LEVELS FOR 1 INTERESTING PARAMETER ($\Delta\chi^2 = 2.7$).

| Parameter | <i>Chandra</i> Value | <i>XMM-Newton</i> Value |
|------------------|---------------------------------------|--------------------------------------|
| $N_{H,Gal}^a$ | (1.3×10^{20}) | (1.3×10^{20}) |
| $N_{H,1}$ | $3.2^{+10.2}_{-3.2} \times 10^{20}$ | (3.2×10^{20}) |
| $N_{H,2}$ | - | $3.6^{+0.6}_{-0.6} \times 10^{21}$ |
| kT_{rs} (keV) | $1.24^{+0.53}_{-0.18}$ | (1.24) |
| $Z(Z_{\odot})$ | (1.0) | (1.0) |
| K_{rs}^b | $2.7^{+1.3}_{-1.0} \times 10^{-6}$ | $2.2^{+4.3}_{-2.2} \times 10^{-6}$ |
| Γ^c | - | $1.88^{+0.13}_{-0.12}$ |
| N_{pl}^d | - | $3.5^{+0.4}_{-0.3} \times 10^{-5}$ |
| kT_{dbb} (keV) | - | $0.20^{+0.11}_{-0.05}$ |
| K_{dbb}^e | - | $4.5^{+2.7}_{-4.4}$ |
| χ^2/dof | 0.88(4.4/5) | 0.98(67.7/69) |
| $f_{0.3-10}^f$ | $0.4^{+0.2}_{-0.2} \times 10^{-14}$ | $15.4^{+1.0}_{-1.0} \times 10^{-14}$ |
| $L_{0.3-10}^g$ | $0.03^{+0.01}_{-0.01} \times 10^{39}$ | $2.1^{+0.2}_{-0.2} \times 10^{39}$ |

^aFrom Kalberla et al. (2005). Units of cm^{-2} .

^bRaymond-Smith model normalization $K_{rs} = 10^{-14}/\{4\pi [d_A (1+z)]^2\} \int n_e n_H dV$, where d_A is the angular size distance to the source (cm), n_e is the electron density (cm^{-3}), and n_H is the hydrogen density (cm^{-3}).

^cPhoton index.

^dUnits of photons $keV^{-1} cm^{-2} s^{-1}$, at 1 keV.

^e $K_{dbb} = [R_{in}(km)/d(10 kpc)]^2 \times \cos\theta$ where R_{in} is the apparent inner-disk radius and θ the viewing angle; $\theta = 0$ is face-on.

^fObserved flux in the 0.3–10 keV band; units of $erg cm^{-2} s^{-1}$.

^gUnabsorbed luminosity in the 0.3–10 keV band; units of $erg s^{-1}$.

and *XMM-Newton* exposures. In summary, X5 appears to be a typical power-law ULX, perhaps powered by accretion onto a BH with a mass $\lesssim 50M_{\odot}$.

6. CONCLUSIONS

We have studied the nature of the five brightest sources in NGC 4631, using *XMM-Newton* and *Chandra* data. Four of them can be classified as ULXs. The most peculiar ULX, which we label X1, was previously studied by Carpano et al. (2007) and identified as a variable supersoft source with an apparent bolometric luminosity $\approx 3 \times 10^{40} erg s^{-1}$. We re-examined the spectral data and found that in fact, its most likely luminosity may be only $\approx 4 \times 10^{39} erg s^{-1}$; in fact, it could be even lower, if we consider that a blackbody approximation tends to overestimate the luminosity of supersoft sources. This reduces the need for an intermediate-mass BH or other exotic scenarios.

We found that when the source is in a low state (*Chandra* observation), it appears soft (but not supersoft), consistent with a thermal spectrum at a temperature ~ 0.1 – 0.3 keV, and a luminosity $10^{37} \lesssim L_{bol} \lesssim 10^{38} erg s^{-1}$.

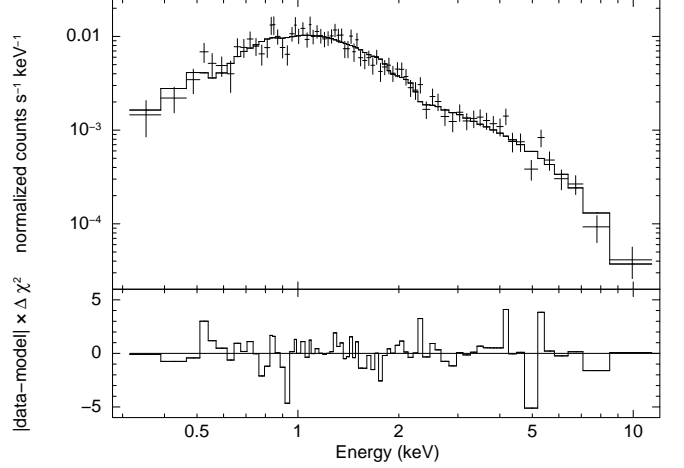


FIG. 9.— *XMM-Newton*/EPIC spectrum of X4 (datapoints and χ^2 residuals), fitted with a disk-blackbody plus power-law model; see Table 6 for the best-fitting parameters.

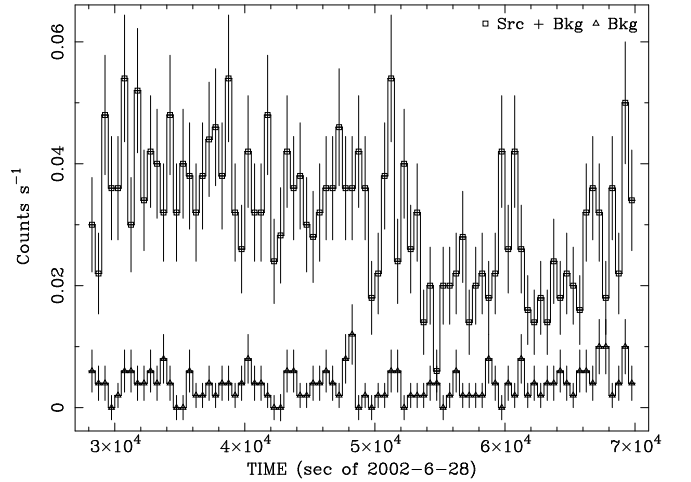


FIG. 10.— *XMM-Newton*/EPIC lightcurve of X4, and corresponding background count rate, showing significant (aperiodic) short-term variability.

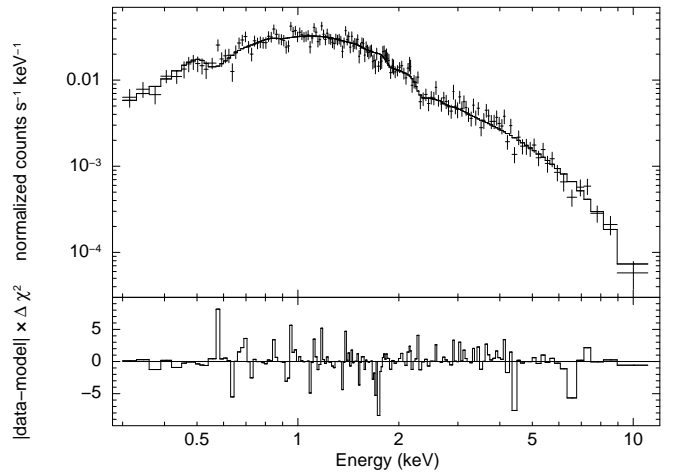


FIG. 11.— *XMM-Newton*/EPIC spectrum of X5 (datapoints and χ^2 residuals), fitted with a simple power-law model; see Table 7 for the best-fitting parameters.

TABLE 7
BEST-FITTING PARAMETERS FOR THE *Chandra*/ACIS AND *XMM-Newton*/EPIC SPECTRA OF X5. SPECTRAL MODEL: `wabs*wabs*power-law`. VALUES IN BRACKETS WERE FIXED. ERRORS ARE 90% CONFIDENCE LEVELS FOR 1 INTERESTING PARAMETER ($\Delta\chi^2 = 2.7$).

| Parameter | <i>Chandra</i> Value | <i>XMM-Newton</i> Value |
|-------------------------------|-------------------------------------|-------------------------------------|
| $N_{\text{H,Gal}}^{\text{a}}$ | (1.3×10^{20}) | (1.3×10^{20}) |
| N_{H} | $2.0^{+0.2}_{-0.2} \times 10^{21}$ | $2.5^{+0.2}_{-0.2} \times 10^{21}$ |
| Γ^{b} | $1.79^{+0.08}_{-0.08}$ | $2.12^{+0.06}_{-0.03}$ |
| N_{pl}^{c} | $8.6^{+0.7}_{-0.7} \times 10^{-5}$ | $13.7^{+0.8}_{-0.7} \times 10^{-5}$ |
| χ^2/dof | 0.95(140.0/147) | 1.13(187.1/166) |
| $f_{0.3-10}^{\text{d}}$ | $4.2^{+0.2}_{-0.3} \times 10^{-13}$ | $4.4^{+0.3}_{-0.2} \times 10^{-13}$ |
| $L_{0.3-10}^{\text{e}}$ | $3.8^{+0.1}_{-0.1} \times 10^{39}$ | $5.0^{+0.2}_{-0.2} \times 10^{39}$ |

^aFrom Kalberla et al. (2005). Units of cm^{-2} .

^bPhoton index.

^cUnits of photons $\text{keV}^{-1} \text{cm}^{-2} \text{s}^{-1}$, at 1 keV.

^dObserved flux in the 0.3–10 keV band; units of $\text{erg cm}^{-2} \text{s}^{-1}$.

^eUnabsorbed luminosity in the 0.3–10 keV band; units of erg s^{-1} .

We argued that this is inconsistent with an intermediate-mass BH. It is also unusual for a stellar-mass BH, which at those luminosities is expected to be in a power-law dominated low/hard state, or in a disk-dominated high/soft state with $T_{\text{in}} \sim 0.5\text{--}1$ keV, based on our current knowledge of canonical accretion states. As an alternative, we suggest that transient super-Eddington outbursts (fireball or photospheric expansion) powered by non-steady nuclear burning on the surface of a massive white dwarf could be a viable scenario, as an extreme subclass of supersoft sources. Outbursts due to photospheric expansion are expected when the accretion rate exceeds $\approx 10^{-6}M_{\odot} \text{yr}^{-1}$. Based on the sequence of available observations from 1991–2002, the long-term average luminosity of the system is $\approx (1\text{--}2) \times 10^{39} \text{erg s}^{-1}$, which requires average accretion rates $\approx (5\text{--}10) \times 10^{-6}M_{\odot} \text{yr}^{-1}$. Although very high, such rates are achievable during phases of thermal-timescale mass transfer in B stars, and are similar to the rates required to explain the most luminous ULXs powered by BH accretion. Hence, we speculate that transient outbursts in nuclear-burning, massive white dwarfs may also explain the few other supersoft ULXs (all highly variable) found in nearby galaxies. Some of those sources would be seen as quasi-soft sources

(in the definition of Di Stefano & Kong 2004) when they are in a low state.

The origin of the 4-hr X-ray variability remains unexplained, whatever the nature of the compact object. Given the high mass transfer rate, we would expect a B-type donor star filling its Roche lobe; however, a 4-hr period does not allow for massive donors. Alternatively, the variability may be due to an accretion disk precession, or the rotation of the white dwarf, or β -Cephei pulsations in the donor star.

The other four brightest sources in NGC 4631 are almost certainly *bone fide* BHs, in different accretion states. X2 ($L_{\text{X}} \approx 3 \times 10^{39} \text{erg s}^{-1}$ in the *XMM-Newton* observation) is a highly absorbed ‘‘convex-spectrum’’ ULX; its X-ray spectrum may be interpreted as emission from a slim disk, or from a low-temperature (a few keV) Comptonizing region. X3 ($L_{\text{X}} \approx 4 \times 10^{38} \text{erg s}^{-1}$) is a stellar-mass BH in its classical disk-dominated high/soft state. X4 ($L_{\text{X}} \approx 3 \times 10^{39} \text{erg s}^{-1}$) is a transient power-law ULX with a soft-excess at $kT \approx 0.20$ keV; for this class of objects, we may be seeing a standard disk outside a transition radius, completely replaced or covered by a Comptonizing region at smaller radii. X5 ($L_{\text{X}} \approx 5 \times 10^{39} \text{erg s}^{-1}$) is a pure power-law ULX, with no evidence for low-energy soft excess or high-energy steepening. All of them are consistent with accreting stellar-mass BHs, with masses $\lesssim 50M_{\odot}$. However, the relation between the different phenomenological states (high/soft, convex-spectrum, power-law, power-law with soft excess), and in particular whether those states are uniquely a function of the normalized accretion rate, remains a topic for further theoretical and observational investigations.

We thank the referee for a thoughtful review and interesting suggestions which have considerably improved the paper. This research has made use of the NASA/IPAC Extragalactic Database (NED) which is operated by the Jet Propulsion Laboratory, California Institute of Technology, under contract with NASA; and from the *Chandra* Data Archive, part of the *Chandra* X-Ray Observatory Science Center (CXC) which is operated for NASA by SAO. Support for this research was provided in part by NASA under Grant NNG04GC86G issued through the Office of Space Science and from the Space Telescope Science Institute under the grant HST/AR-10954. RS acknowledges support from a Leverhulme Fellowship, a UK-China Fellowship for excellence, and from Tsinghua University (Beijing). We thank Kinwah Wu, Shaung-Nan Zhang, Xin-Lin Zhou for their comments and discussions.

REFERENCES

- Arnaud, K. A. 1996, *Astronomical Data Analysis Software and Systems V*, ASP Conference Series Vol. 101, G. H. Jacoby and J. Barnes eds, 17
- Begelman, M. C. 2002, *ApJ*, 568, L97
- Begelman, M. C. 2006, *ApJ*, 643, 1065
- Berghöfer, T. W., Vennes, S., & Dupuis, J. 2000, *ApJ*, 538, 854
- Boller, Th., Tanaka, Y., Fabian, A., Brandt, W. N., Gallo, L., Anabuki, N., Haba, Y., & Vaughan S. 2003, *MNRAS*, 343, L89
- Callanan, P. J., Machin, G., Naylor, T., & Charles, P. A. 1989, *MNRAS*, 241, 37
- Carpano, S., Pollock, A. M. T., King, A. R., Wilms, J., & Ehle, M. 2007, *A&A*, 471, L55
- Carpano, S., Wilms, J., Schirmer, M., & Kendziorra, E. 2006, *A&A*, 458, 747
- Cash, W. 1979, *ApJ*, 228, 939
- Di Stefano, R., & Kong, A. K. H. 2004, *ApJ*, 609, 710
- Fabbiano, G., King, A. R., Zezas, A., Ponman, T. J., Rots, A., & Schweizer, F. 2003, *ApJ*, 591, 843
- Fabbiano, G., Kim, D.-W., & Trinchieri, G. 1992, *ApJS*, 80, 531
- Feng, H., & Kaaret, P. 2005, *ApJ*, 633, 1052
- Finley, J. P., Belloni, T., & Cassinelli, J. P. 1992, *A&A*, 262, L25
- Gierliński, M., & Done, C. 2004, *MNRAS*, 347, 885
- Grimm, H.-J., Gilfanov, M., & Sunyaev, R. 2003, *MNRAS*, 339, 793

- Iben, I. J., & Tutukov, A. V. 1994, *ApJ*, 431, 264
- Kalberla, P. M. W., Burton, W. B., Hartmann, D., Arnal, E. M., Bajaja, E., Morras, R., & Poppel, W. G. L. 2005, *A&A*, 440, 775
- Kahabka, P. 2004, *A&A*, 416, 57
- Kahabka, P., & van den Heuvel, E. P. J. 1997, *ARA&A*, 35, 69
- Kennicutt, R. C. 1998, *ARA&A*, 36, 189
- King, A. R. 2008, *MNRAS*, 385, L113
- King, A. R., Davies, M. B., Ward, M. J., Fabbiano, G., & Elvis, M. 2001, *ApJ*, 552, L109
- Kong, A. K. H., & Di Stefano, R. 2003, *ApJ*, 590, L13
- Kong, A. K. H., & Di Stefano, R. 2005, *ApJ*, 632, 107L
- Liu, J.-F., & Bregman, J. N. 2005, *ApJSS*, 157, 59
- Makishima, K. 2007, *IAU Symposium*, 238, 209
- Makishima, K., et al. 2000, *ApJ*, 535, 632
- Miller, M. C., & Colbert, E. J. M. 2004, *IJMPD*, 13, 1
- Ohsuga, K., & Mineshige, S. 2007, *ApJ*, 670, 1283
- Page, M. J., Davis, S. W., & Salvi, N. J. 2003, *MNRAS*, 343, 1241
- Pakull, M. W., & Mirioni, L. 2002, in the unpublished proceedings of the symposium “New visions of the X-ray Universe in the *XMM-Newton* and *Chandra* era”, ESTEC, The Netherlands (November 2001), astro-ph/0202488
- Poutanen, J., Lipunova, G., Fabrika, S., Butkevich, A. G., & Abolmasov, P. 2007, *MNRAS*, 377, 1187
- Rappaport, S. A., Podsiadlowski, Ph., & Pfahl, E. 2005, *MNRAS*, 356, 401
- Read, A. M., Ponman, T. J., & Strickland, D. K. 1997, *MNRAS*, 286, 626
- Schwarz, G. J., Shore, S. N., Starrfield, S., Hauschildt, P. H., Della Valle, M., & Baron, E. 2001, *MNRAS*, 320, 103
- Seth, A. C., Dalcanton, J. J., & de Jong, R. S. 2005, *AJ*, 129, 1331
- Shafee, R., McClintock, J. E., Narayan, R., Davis, S. W., Li, L.-X., & Remillard, R. A. 2006, *ApJ*, 636, L113
- Shakura, N. I., & Sunyaev, R. A. 1973, *A&A*, 24, 337
- Shimura, T., & Takahara, F. 1995, *ApJ*, 445, 780
- Soifer, B. T., Boehmer, L., Neugebauer, G., & Sanders, D. B. 1989, *AJ*, 98, 766
- Soria, R., & Kuncic, Z. 2008, to appear in the proceedings of the conference “Observational evidence of black holes”, Kolkata, India (February 2008), arxiv:0807.0016
- Stankov, A., & Handler, G. 2005, *ApJS*, 158, 193
- Starrfield, S., Timmes, F. X., Hix, W. R., Sion, E. M., Sparks, W. M., & Dwyer, S. J., 2004, *ApJ*, 612, L53
- Stobbart, A.-M., Roberts, T. P., & Wilms, J. 2006, *MNRAS*, 368, 397
- Strickland, D. K., Heckman, T. M., Colbert, E. J. M., Hoopes, C. G., & Weaver, K. A. 2004b, *ApJS*, 151, 193
- Strickland, D. K., Heckman, T. M., Colbert, E. J. M., Hoopes, C. G., & Weaver, K. A. 2004b, *ApJ*, 606, 829
- Swartz, D. A., Ghosh, K. K., Suleimanov, V., Tennant, A. F., & Wu, K. 2002, *ApJ*, 574, 382
- Swartz, D. A., Ghosh, K. K., Tennant, A. F., & Wu, K. 2004, *ApJS*, 154, 519
- Tennant, A. F. 2006, *AJ*, 132, 1372
- Tüllmann, R., Pietsch, W., Rossa, J., Breitschwerdt, D., & Dettmar, R. J. 2006, *A&A*, 448, 43
- Tüllmann, R., Breitschwerdt, D., Rossa, J., Pietsch, W., & Dettmar, R. J. 2006, *A&A*, 457, 779
- Vogler, A., & Pietsch, W. 1996, *A&A*, 311, 35
- Wang, Q. D., Immler, S., Walterbos, R., Lauroesch, J. T., & Breitschwerdt, D. 2001, *ApJ*, 555, L39
- Warner, B. 1995, *Ap&SS*, 232, 89
- Watarai, K.-Y., Mizuno, T., & Mineshige, S. 2001, *ApJ*, 549, L77
- Winter, L. M., Mushotzky, R. F., & Reynolds, C. S. 2006, 649, 730
- Winter, L. M., Mushotzky, R. F., & Reynolds, C. S. 2007, *ApJ*, 655, 163